Crystal Structure of a pH-Stabilized Mutant of Villin Headpiece[†]

Jianmin Meng[‡] and C. James McKnight*

Department of Physiology and Biophysics, Boston University School of Medicine, Boston, Massachusetts 02118

Received November 14, 2007; Revised Manuscript Received February 1, 2008

ABSTRACT: Villin-type headpiece domains are compact F-actin-binding motifs that have been used extensively as a model system to investigate protein folding by both experimental and computational methods. Villin headpiece (HP67) harbors a highly helical, thermostable, and autonomously folding subdomain in the C terminus (HP35), and because of this feature, HP67 is usually considered to be composed of a N- and C-terminal subdomain. Unlike the C-terminal subdomain, the N-terminal subdomain consists mainly of loops and turns, and the folding is dependent upon the presence of the C-terminal subdomain. The pH sensitivity of this subdomain is thought to arise from, at least partially, protonation of H41 buried in the hydrophobic core. Substitution of this histidine with tyrosine, another permissive residue at this position for naturally occurring sequences, increases not only the pH stability of HP67 but also the thermal stability and the cooperativity of thermal unfolding over a wide pH range (0.9–7.5). The crystal structures of wild-type HP67 and the H41Y mutant, determined under the same conditions, indicate that the H41Y substitution causes only localized rearrangement around the mutated residue. The F-actin-binding motif remains essentially the same after the mutation, accounting for the negligible effect of the mutation on F-actin affinity. The hydrogen bond formed between the imidazole ring of H41 and the backbone carbonyl of E14 of HP67 is eliminated by the H41Y mutation, which renders the extreme N terminus of H41Y more mobile; the hydrogen bond formed between the imidazole ring of H41 and the backbone nitrogen of D34 is replaced with that between the hydroxyl group of Y41 and the backbone nitrogen of D34 after the H41Y substitution. The increased hydrophobicity of tyrosine compensates for the loss of hydrogen bonds in the extreme N terminus and accounts for the increased stability and cooperativity of the H41Y mutant.

Villin-type headpiece domains are motifs found at the extreme C termini of a variety of cytoskeleton-related proteins. They are compact, containing about 70 amino acids. Villin headpiece is the first defined and most extensively studied domain in the headpiece family. It provides the second F-actin-binding site required for the F-actin-bundling activity of villin (*1*).

A construct containing the C-terminal 67 residues of chicken villin headpiece (HP67)[1] retains full F-actin-binding activity (*2*) and has been used to determine both its nuclear magnetic resonance (NMR) and crystal structure (*3, 4*). HP67 is composed of two subdomains that share an extended hydrophobic core. The N-terminal subdomain (residues 10–41) contains mainly loops and turns, with only a few residues in short α or 3–10 helices. Residues 20–30 form a loop that varies in length among different headpiece domain sequences (V loop) (*4*). The N-terminal subdomain is unstructured in isolation. In comparison, the C-terminal subdomain of villin headpiece (HP35, residues 42–76) is thermostable and folds autonomously in a few microseconds (*5–7*). It is composed of three α helices that are also the major helical components of HP67 (*3, 4*). HP35 has been widely used as a model system to probe protein folding in both theoretical and experimental fields.

Mutational studies have shown that residues R37, K38, and E39 in the N-terminal domain and residues W64, K65, K70, K71, L75, and F76 in the last helix of the C-terminal subdomain contribute to actin-binding by villin headpiece (*3, 8–10*). With the exception of E39 and K70 that form a buried salt bridge, these residues form a contiguous binding surface composed of a "hydrophobic cap" (W64), a "charged crown" (R37, K65, K71, and the carboxylate of the C-terminal F76), and a positively charged "patch" (K38) (*3, 4*). By itself, HP35, which contains most of the residues implicated in F-actin binding, however, does not bind F-actin with high affinity (*2, 10*). This could be due to the exclusion of R37 and K38, two positively charged residues that contribute to the basic charge to the surface (*3*), and/or the alternative conformation and increased flexibility of the two C-terminal residues, L75 and F76 (*11–13*), in the HP35 structure. Thus, a folded N-terminal subdomain can influence

[†] This work is supported by National Institutes of Health (NIH) Grant GM62886 to C.J.M.

* To whom correspondence should be addressed. Telephone: 617-638-4042. Fax: 617-638-4041. E-mail: cjmck@bu.edu.

[‡] Current address: Division of Infectious Diseases and Immunology, University of Massachusetts Medical School, Worcester, MA 01605.

[1] Abbreviation: B_{max}, maximal binding constant; CD, circular dichroism; HP67, villin headpiece (from residues 10–76); HP35, villin headpiece C-terminal subdomain (from residues 42–76); K_d, equilibrium dissociation constant; NMR, nuclear magnetic resonance; PEG, polyethylene glycol; rmsd, root-mean-square deviation; SAS, solvent-accessible surface; T_m, thermal unfolding midpoint; ΔT_m, difference in the thermal unfolding midpoints.

10.1021/bi7022738 CCC: $40.75
Published on Web 03/28/2008

F-actin binding directly by providing the basic cluster and indirectly by stabilizing the conformation of the C-terminal subdomain.

In the HP67 structure, there is a buried histidine (H41) in the N-terminal hydrophobic core (*3, 4*). In the folded state at pH 7, the histidine imidazole ring is uncharged and involved in two hydrogen bonds. H41 acts as a pH-sensitive switch for the folding of the N-terminal subdomain. Unfolding of the N-terminal subdomain begins when the pH is dropped below pH ~6, while the C-terminal subdomain remains folded. The apparent pK_a of H41 is lowered by 1 pH unit from free histidine (5.0 versus 6.0, respectively). This apparent pK_a represents neither the pK_a of H41 in the folded or unfolded state (*14*). Instead, the apparent pK_a of H41 is lower than that of the unfolded state, which should be close to free histidine (*4*), but higher than histidine in the fully folded state, which has been calculated to have a pK_a of 3.2 (*16*).

In known headpiece sequences, tyrosine is the only other residue that occupies this position (*2*). It is similar to histidine in shape and size but is more hydrophobic and the hydroxyl group does not titrate at low pH. The point-mutant H41Y was created to examine the role of H41 in pH-induced unfolding of villin headpiece (*15, 16*). By following the fingerprint NMR chemical shifts of individual subdomains, Raleigh and co-workers demonstrated that unfolding of HP67 is a multistate process and the unfolding of the N-terminal subdomain preceeds that of the C-terminal subdomain (*15*). The H41Y substitution stabilizes both domains, but the N-terminal subdomain is still less stable than the C-terminal subdomain (*15*). Using ^{15}N-relaxation dispersion experiments, Palmer and co-workers further demonstrated that the unfolding of the N-terminal subdomain occurs through a partially folded intermediate involving residual interactions with the imidazole ring of H41 (*16*). This intermediate was not observed in the H41Y mutant.

In this study, we continued to use this point-mutant system to extend our knowledge on pH-induced unfolding and to understand the biological relevance and the structural basis. We found that the H41Y substitution increases not only the pH stability but also the thermal stability of HP67 over a wide pH range. The cooperativity of the thermal unfolding curves is also increased by the mutation over the tested pH range, indicating a tighter coupling of the N and C termini after the mutation. The crystal structures of HP67 and H41Y, determined under identical conditions, indicate that the H41Y substitution causes only localized rearrangement in the vicinity of the mutated residue. The F-actin binding motif on the surface remains essentially the same after the mutation, accounting for the negligible effect by the mutation on F-actin affinity. Two hydrogen bonds involving the imidazole ring of H41 are modified by the mutation, resulting in increased flexibility in the extreme N terminus of H41Y. The increased hydrophobicity of tyrosine, however, compensates for the loss of the hydrogen bond to the extreme N terminus and accounts for the increased stability and unfolding cooperativity after the mutation.

MATERIALS AND METHODS

Mutagenesis, Protein Expression, and Purification. The pET24a-based expression vector PVHP10-76 (*4*) was used to express HP67. The mutant H41Y was created by QuikChange mutagenesis under the instructions of the manufacturer (Stratagene). The mutation was confirmed by DNA sequencing (Boston University School of Medicine Molecular Genetic Core Facility).

Proteins were expressed in *Escherichia coli* BL21 (DE3) cells (Novagen) and purified as described previously (*3*). Purified proteins were stored as lyophilized powders. Actin was purified from chicken pectoral muscle using standard procedures (*3, 4, 17*). The G-actin concentration was determined by absorbance at 290 nm using an extinction coefficient of 26640 L M^{-1} cm^{-1}. The concentrations of headpiece mutants were determined by absorbance at 280 nm using extinction coefficients of 5690 and 6970 L M^{-1} cm^{-1} for HP67 and H41Y, respectively (*18*). The concentration measurements for G-actin and headpiece proteins were taken after 1 h of ultracentrifugation (100000*g*) at 4 °C immediately before each experiment.

Circular Dichroism (CD) Measurements. CD spectra were acquired on an Aviv 62DS spectrometer. Samples contained 20 μM protein in 1 mM borate, 1 mM citrate, and 1 mM phosphate, with the pH adjusted from 8 to 1 with HCl and NaOH. The exact pH value of each sample was determined right after each experiment. The data points for the thermal unfolding experiments were collected at 222 nm, with 25 s of signal averaging at 2° intervals from 0 to 100 °C after a 60 s temperature equilibration time in a 2 mm path-length cell. The melting temperatures (T_m) were derived from the first derivative of the melting curve using Origin 6.0 (Microcal Software, Inc., Northampton, MA).

Actin Sedimentation Assay. Sedimentation assays were performed at 4 °C as described previously (*3*). F-Actin (40 μM) was incubated with the 0, 5, 10, 25, 50, 100, or 200 μM headpiece domain for 1 h at 4 °C before sedimentation at 100000*g* for 1 h. After removal of the supernatant, the pellets were washed with F-buffer (10 mM Tris-HCl at pH 8.0, 1 mM $MgCl_2$, 100 mM NaCl, 0.1 mM ATP, 0.2 mM DTT, 3 mM NaN_3, and 0.1 mM $CaCl_2$) once and resedimented at 100000*g* for 10 min. Fractions containing bound proteins were separated on tricine gels and stained with Coomassie Blue (*19, 20*). The gels were quantified on a Bio-Rad GS-700 imaging densitometer. Two binding parameters, the equilibrium dissociation constant (K_d) and maximal binding constant (B_{max}) were obtained by fitting the data in Origin 6.0 (Microcal Software, Inc., Northampton, MA) (*3*).

Crystallization, X-ray Diffraction Data Collection, and Structure Determination. Initial crystallization conditions were identified with a sparse matrix crystal screen (Crystal Screen, Hampton Research, Laguna Niguel, CA). Hanging droplets consisting of 2 μL of protein stock solution (30 mg/mL in pure water) mixed with 2 μL of the reservoir solution were equilibrated against 0.5 mL of reservoir solution consisting of 0.2 M ammonium sulfate, 0.1 M 2-morpholinoethanesulfonic acid (pH 6.5), and 30% polyethylene glycol (PEG) 8000. Crystallization was optimized by microseeding with a reduced protein concentration (15 mg/mL) and a reduced precipitant concentration (PEG 8000, 25%). Rod-shaped crystals grew within 3 days at room temperature to ~300 μM maximum dimension.

The crystals were then cryoprotected by soaking sequentially in reservoir solutions containing 10% glycerol followed by 20% glycerol for 3 min each. The crystals were then

Table 1: Crystallographic Statistics of HP Mutant

Statistics of Data Collection and Processing		
	HP67	H41Y
X-ray source	Raxis IV	Raxis IV
space group	$P2_12_12_1$	$P2_12_12_1$
cell axes (Å)	31.212, 37.780, 53.147	31.419, 38.259, 52.807
cell angles (deg)	90, 90, 90	90, 90, 90
resolution limit (Å)	1.40	1.50
redundancy (total/unique)	5.5 (69 211/12 685)	6.2 (61 575/9864)
R_{sym}[a] (%), overall (final shell)	4.4 (18.5)	6.1 (8.8)
completeness (%), overall (final shell)	97.7 (92.5)	92.3 (86.8)
I/σ_I, overall (final shell)	34.3 (5.6)	28.2 (17.2)

Statistics of Model Refinement		
nonhydrogen atoms		
protein	514	539
water	82	124
R_{cryst}[b] (%)	20.9	18.0
R_{free}[c] (%)	23.3	20.6
rmsd		
bond length (Å)	0.008	0.008
bond angles (deg)	1.38	1.35
averaged B values (Å^2)		
main chain	14.53	9.62
side chain	17.48	11.74
water	24.3	20.68
Ramachandran plot (%)		
most favored	96.4	96.6
additionally allowed	3.6	3.4
disallowed	0	0

[a] $R_{sym} = \sum_h\sum_i|I_{hi} - I_h|/\sum_h\sum_i I_{hi}$ for the intensity (i) of i observations of reflection h. [b] $R_{crys} = \sum||F_{obs}| - |F_{calc}||/\sum|F_{obs}|$, where F_{obs} and F_{calc} are the observed and calculated structure factor amplitudes, respectively. [c] R_{free} was calculated as R_{cryst} but with 8% of the amplitudes chosen randomly and omitted from the start of refinement.

immediately frozen under N_2 vapor at 95 K. Diffraction data were collected on a RAXIS IV (Boston University School of Medicine). The data were processed with the HKL suite (HKL Research, Inc.). The structures were determined by molecular replacement using the phases from our previously determined crystal structure, 1YU5 (*3*). Electron-density maps were calculated at 1.4 and 1.5 Å for HP67 and H41Y, respectively. The structures were modeled using O (*21*) and refined using torsional dynamics and the maximum likelihood target function in CNS (*22*). The structural statistics are summarized in Table 1. The coordinates have been deposited in the Research Collaboratory for Structural Bioinformatics (RCSB) protein database under the accession codes 2RJY and 2RJV for HP67 and H41Y, respectively.

RESULTS

Replacement of Histidine 41 with Tyrosine Increases Protein Stability. Far-UV CD spectra were collected as a function of pH to test whether the histidine to tyrosine mutation results in stabilization of H41Y relative to HP67. The CD signal at 222 nm is of greater magnitude for H41Y because of the introduction of the tyrosine aromatic ring (*3, 23, 24*). When the far-UV CD signal at 222 nm is plotted against pH at a constant temperature of 55 °C (Figure 1a), the unfolding curve for H41Y is shifted to lower pH by

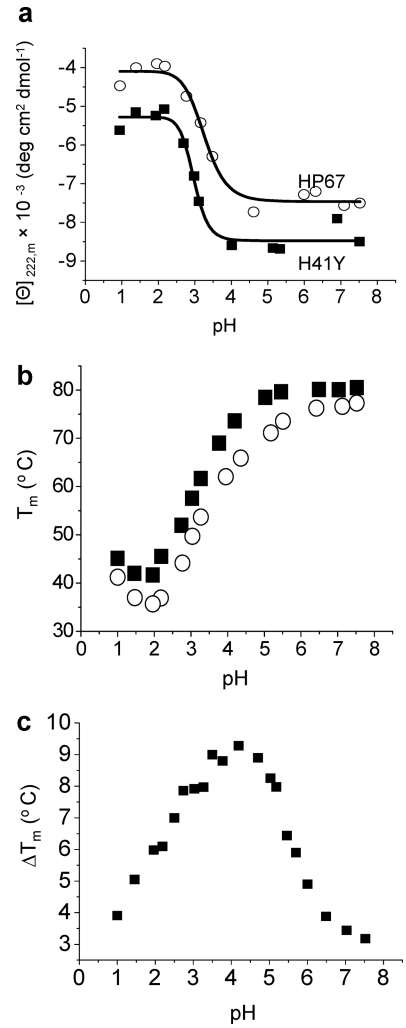

FIGURE 1: pH stabilization by the H41Y mutation in HP67. (a) Far-UV CD signal at 222 nm of HP67 (○) and H41Y (■) at 55 °C is shown as a function of pH. The solid lines are the best fit to a sigmoidal function. (b) Thermal unfolding midpoints (T_m) of HP67 (○) and H41Y (■) monitored by the CD signal at 222 nm are plotted as a function of pH. (c) Difference in T_m of H41Y versus HP67 is plotted as a function of pH. In a−c, samples contained 20 μM protein in 1 mM borate, 1 mM citrate, and 1 mM phosphate buffer in a 1 or 2 mm path-length cell. The pH was adjusted by the addition of HCl and NaOH.

0.3 pH unit (3.0 for H41Y versus 3.3 for HP67). Because the major source of the CD signal at 222 nm is the three α helices in the C terminus, this stabilization reflects changes in the C-terminal subdomain from a mutation in the N-terminal hydrophobic core. Although unfolding of HP67 is not a two-state process, the calculation of apparent thermal unfolding midpoint (T_m) allows for a qualitative comparison of the thermal stability between the two constructs (*15*).

Thermal unfolding experiments were monitored by CD at 222 nm over a pH range of 1−8 (Supplementary Figure 1 in the Supporting Information). H41Y unfolds more cooperatively over most of this range and always with a higher T_m (Figure 1b). At very low pH (i.e., pH 0.9), where all acidic groups are expected to be protonated, including the C terminus, the cooperativity of the unfolding curves is similar but H41Y is still 4 °C more thermostable than HP67. Even at this low pH, there is significant cooperatively folded structure in both HP67 and H41Y.

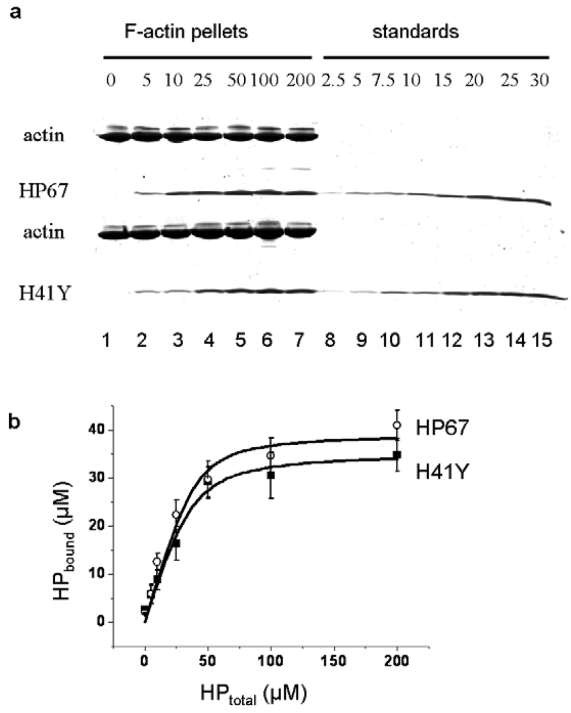

FIGURE 2: H41Y mutation does not alter F-actin-binding activity. (a) Representative gels of the F-actin sedimentation assay. Lanes 1–7, 40 μM F-actin was incubated with the concentration of headpiece domain indicated above each lane for 1 h at 4 °C before sedimentation at 100000*g* for 1 h. Lanes 8–15 are peptide standards run to aid in quantifying the amount of protein cosedimenting with F-actin. The bands corresponding to actin and the respective headpiece domains are labeled. (b) Quantitation of the F-actin sedimentation assay. The concentration of the headpiece domains cosedimenting with F-actin are plotted against the total headpiece concentration in each reaction. The data points are the average of four separate experiments, and the error bars indicate the standard deviations of the four experiments. The curves are the best fit to the average data points HP67 (○) and H41Y (■).

The most pronounced difference in T_m is within the transition region (pH 5.5–3.0), where the T_m difference is 6–10 °C (parts b and c of Figure 1). The T_m of H41Y remains essentially the same until the pH drops below 5.5, whereas the T_m of HP67 drops below pH 7. A trough in the T_m versus pH curve is observed for both constructs near pH 2.0 (Figure 1b) that might reflect a stabilizing effect of the protonation of the C-terminal carboxyl groups. Thus, the H41Y mutation stabilizes HP67 to thermal unfolding over the entire tested pH range.

H41Y Mutation Preserves F-Actin Affinity. F-Actin sedimentation assays were performed to measure the impact of the H41Y mutation on F-actin affinity. Figure 2a shows representative gels of the sedimentation assays used to measure the binding of both constructs. The amount of H41Y peptide cosedimented with F-actin is comparable to that of HP67, indicating that H41Y has similar affinity for F-actin as HP67. Two binding parameters, the maximal binding constant (B_{max}) and the equilibrium dissociation constant (K_d), were obtained by fitting the data to the formalism of Swillens et al. (*25*) (Figure 2b). The B_{max} values of 39.2 ± 2.7 and 35.3 ± 2.0 μM for HP67 and H41Y, respectively, are close to each other and the 40 μM F-actin concentration initially included in the reactions, indicating a 1:1 protein/actin-binding ratio. The K_d values (4.4 ± 2.8 μM for HP67 and 6.4 ± 2.8 μM for H41Y) remain essentially unchanged by the mutation, confirming the minimal effect of this mutation on F-actin affinity. Thus, at neutral pH, where the sedimentation assays were performed, the H41Y substitution does not affect the F-actin-binding affinity of villin headpiece.

H41Y Mutation Causes Only Localized Structural Changes. To understand the structural basis for the increased stability and the negligible effect on F-actin affinity, we determined the high-resolution crystal structures of HP67 and H41Y under identical conditions. This condition is slightly different from the one that we used earlier to crystallize wild-type HP67 (*3*). Instead of high salt, PEG 8000 was used as the precipitant. Microseeding was used to optimize crystallization. Both constructs crystallize in space group $P2_12_12_1$, with one molecule in the asymmetric unit, as previously reported (*3*) (see Table 1 for structural statistics). The structure of HP67 crystallized from PEG 8000 is virtually identical to that previously determined in high salt, with a backbone root-mean-square deviation (rmsd) for residues 13–76 of 0.113 Å for the backbone and 0.601 Å for all heavy atoms. For the region of the thermostable subdomain (residues 42–76), the rmsd is even lower: 0.039 Å for the backbone and 0.545 Å for all heavy atoms.

As shown in Figure 3a, the crystal structure of H41Y is essentially identical to that of HP67. The rmsd is 0.405 Å for the backbone atoms and 0.845 Å for all atoms, omitting the mutated residue and residues 10–12 that have poor electron density in the HP67 structure. After alignment of the backbones, the two residues at the mutation site, H41 and Y41, overlay with each other well. The largest difference between the two structures is in the residues at the extreme N termini. The V loop, is displaced slightly from the hydrophobic core to accommodate the extra hydroxyl group of tyrosine. The F-actin-binding motif remains essentially the same after the mutation (Figure 3b).

Modifications of the Hydrogen Bonds adjacent to Residue 41. At neutral pH, H41 in HP67 populates the δ-tautomer conformation (*15, 16, 26*) that allows the formation of two hydrogen bonds: the δ1 proton hydrogen bonds to the backbone carbonyl oxygen of E14, and the nitrogen at the ε2 position hydrogen bonds to the backbone amide proton of D34 (Figure 4a). A hydrogen bond is also observed between the main-chain carbonyl oxygen of H41 and the amide proton of F16 that further restrains the position of residue 41. When the pH is dropped and the imidazole ring is protonated, the hydrogen bond to D34 is lost and a positive charge would be introduced into the hydrophobic core.

The substitution of H41 with tyrosine results in the loss of the hydrogen bond to the backbone of E14 and a modified hydrogen bond to D34 (Figure 4b). Instead of the nitrogen at the ε2 position from the imidazole ring, the hydroxyl oxygen on the tyrosine ring acts as the hydrogen-bond acceptor for the amide proton of D34. Correspondingly, decreased order parameters, indicating greater motion, were observed for the extreme N terminus of H41Y in the neighborhood of E14 (*16*).

Modifications to the Hydrophobic Core. The substitution of H41 with tyrosine does not disrupt the hydrophobic core (parts c and d of Figure 4). Tyrosine packs well, if not better, to the N-terminal hydrophobic core (Figure 4d). The increased hydrophobicity of tyrosine, as well as a similar ring shape, likely accounts for the tolerance of the mutation.

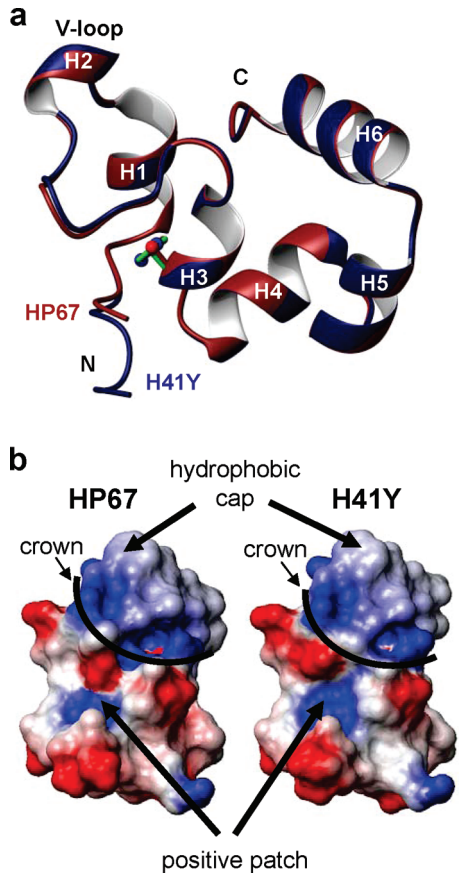

FIGURE 3: Comparison of the crystal structures of HP67 and H41Y. (a) Overlay of the backbone ribbon diagrams of the crystal structures of HP67 (red) and H41Y (blue). The structures are fit to the backbone atoms of residues 14–40 and 42–76. The side chains of H41 and Y41 are shown in orange and green, respectively. Nitrogen and oxygen atoms are shown as blue and red spheres, respectively. The V loop, helices, and the N and C termini are labeled. (b) Comparison of the charged surface potential of the putative actin-binding faces of HP67 (left) and H41Y (right). Blue represents positive charge; red represents negative charge; and white is neutral. The hydrophobic cap, charged crown, and positive patch features of the putative binding face are labeled. Images were produced with MOLMOL (*27*).

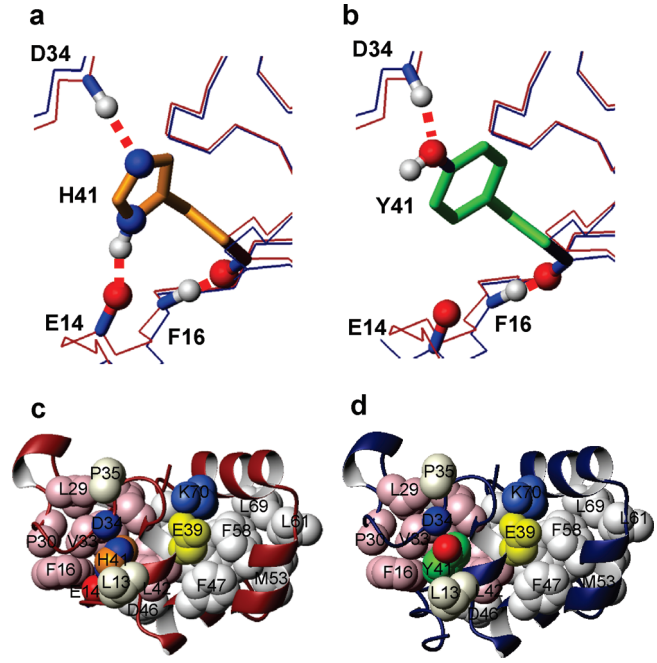

FIGURE 4: Detailed views of the hydrogen bonds and hydrophobic cores of HP67 and H41Y. (a and b) Aligned backbones of HP67 (red) and H41Y (blue). The orientations for both figures are similar to that in Figure 3a. (a) Interactions with H41 (orange) of HP67. (b) Interactions with Y41 (green) from H41Y. Hydrogen bonds are shown as red dashed lines. Hydrogen, nitrogen, and oxygen atoms involved in hydrogen bonds are shown as gray, blue, and red spheres, respectively. Hydrophobic core of (c) HP67 and (d) H41Y. The side chains heavy atoms of residues with 20% or less solvent-accessible surface area are shown as spheres and labeled. Core residues from the N-terminal subdomain (residues 10–41) are pink, and those from the C-terminal subdomain (residues 42–76) are shown in white. Nitrogen and oxygen atoms involved in hydrogen bonding with residue 41 are shown in blue and red, respectively. E39 and K70 that form a salt bridge between the two subdomains are shown in yellow and blue, respectively. Two peripheral residues, L13 and P35, are shown in gray. The views in c and d are slightly rotated from those in a and b. Images were produced with MOLMOL (*27*).

Indeed, when H41 is mutated to cysteine, the protein stability drops dramatically (*8*).

The increased hydrophobic interaction between Y41 and other residues in the N-terminal hydrophobic core may compensate for the loss of the hydrogen bond between H41 and E14 after the mutation. For example, there is more contact between the tyrosine side chain and the aromatic ring of F16 and the aliphatic side chain of L13 (Figure 4d). The solvent-accessible surface (SAS) of F16 decreases from 14.7 to 10.29% after the mutation. Residue L13 also moves closer to the hydrophobic core, decreasing its SAS from 58.8 to 30.2% after the mutation.

DISCUSSION

To test the hypothesis that H41 acts as a sensitive switch for pH-induced unfolding of the N-terminal subdomain of villin headpiece (*4*), we constructed a mutant that replaces H41 with tyrosine (*15, 16*). Tyrosine is close to histidine in size and shape but does not undergo protonation below pH 7.0. Furthermore, tyrosine is the only other residue found at this position in the known headpiece sequences.

By monitoring the NMR chemical shifts for individual residues in both the N- and C-terminal subdomains of HP67 under increasingly denaturing conditions, Tang et al. clearly demonstrated that folding of HP67 is a multistate process (*15*). The N-terminal subdomain unfolds before the C-terminal subdomain whether unfolding is due to lowered pH, thermal unfolding, or chemical denaturation. Replacement of H41 with tyrosine in the H41Y mutant eliminates the pH-dependent unfolding of HP67, but the N-terminal subdomain still unfolds at lower temperature and denaturant concentration than the C-terminal subdomain. Thus, the unfolding of both HP67 and H41Y is "segmental", with the N-terminal subdomain unfolding before the C-terminal subdomain.

Using ^{15}N-relaxation dispersion NMR methods that are sensitive to exchange between folded and unfolded states, Grey et al. show that the N-terminal subdomain of HP67 unfolds through a partially structured intermediate (*16*). The intermediate is structured in the region close in space to H41 in the native state. In the H41Y mutant, this partially structured intermediate in the N-terminal subdomain is not seen. Thus, the formation of the intermediate is dependent upon the presence of the histidine side chain. Unfolding of H41Y, however, is still non-two-state, with the N-terminal subdomain unfolding before the C-terminal subdomain.

Consistent with these reports, we found that the H41Y mutation increases the pH stability, whether judged by the far-UV CD signals over different pH values or the apparent T_m over the entire pH range. In addition, the same mutation increases the cooperativity of thermal unfolding over a wide pH range. The F-actin-binding affinity, however, is not affected by this mutation. In light of these findings, we determined the crystal structures of HP67 and H41Y under identical conditions.

While the mutation has little effect on the overall structure, the detailed packing of the N-terminal hydrophobic core is modified by the mutation, and most noticeably, the two hydrogen bonds involving H41. The first hydrogen bond, formed between the imidazole δ1 proton of H41 and the backbone carbonyl oxygen of E14, is removed by the mutation. Consequently, decreased order was observed in residues L13−F16 of H41Y relative to HP67 by NMR relaxation methods (*16*). However, the overall protein stability of H41Y is not compromised, indicating the presence of compensating interactions in stabilizing this mutant.

The second hydrogen bond, formed between the ε2 nitrogen of H41 and the backbone amide proton of D34, is slightly modified by the mutation. Instead of the ε2 nitrogen, the hydroxyl oxygen from the tyrosine side chain hydrogen bonds to the backbone amide proton of D34. Although this hydrogen bond is conserved between HP67 and H41Y, decreased order was still observed in H41Y for residues close to D34 (residues R31−D34) (*16*). This increase in flexibility is likely due to the loss of the hydrogen bond between H41 and E14. The two hydrogen bonds to H41 may act as a "bridge", restraining the motions of both regions of HP67 relative to H41Y. Thus, the loss of the hydrogen bond to E14 results in increased flexibility in both regions.

A third hydrogen bond involving residue 41, between the backbone carbonyl oxygen of residue 41 and backbone amide proton of F16, is not affected by the mutation. F16, however, is less exposed to the solvent after the H41Y substitution. In light of the difference between histidine and tyrosine, we conclude that the increased hydrophobicity of tyrosine results in the increased hydrophobic interaction in the N-terminal hydrophobic core and counteracts for the loss of the hydrogen bond between H41 and E14. Despite the increased stability of H41Y arising from the increased hydrophobic interaction, residues L13−F16 and R31−D34 still have increased flexibility in H41Y. Thus, hydrogen bonds and hydrophobic interaction are the two major forces in immobilizing and stabilizing the N-terminal subdomain of villin headpiece.

ACKNOWLEDGMENT

We thank Dr. Wilson S. Colucci [Department of Medicine, Boston University Medical Center (BUMC)] for providing densitometer facilities. We thank Dr. Yeming Wang for help with X-ray data collection and structure refinement.

SUPPORTING INFORMATION AVAILABLE

Representative thermal unfolding curves of HP67 and H41Y at differenct pH values. This material is available free of charge via the Internet at http://pubs.acs.org.

REFERENCES

1. Glenney, J. R., Jr., Geisler, N., Kaulfus, P., and Weber, K. (1981) Demonstration of at least two different actin-binding sites in villin, a calcium-regulated modulator of F-actin organization. *J. Biol. Chem. 256*, 8156–8161.
2. Vardar, D., Chishti, A. H., Frank, B. S., Luna, E. J., Noegel, A. A., Oh, S. W., and McKnight, C. J. (2002) Villin-type headpiece domains show a wide range of F-actin-binding affinities. *Cell Motil. Cytoskeleton 52*, 9–21.
3. Meng, J., Vardar, D., Wang, Y., Guo, H., Head, J., and McKnight, C. (2005) High-resolution crystal structures of villin headpiece and mutants with reduced F-actin binding activity. *Biochemistry 44*, 11963–11973.
4. Vardar, D., Buckley, D., Frank, B., and McKnight, C. (1999) NMR structure of an F-actin binding "headpiece" motif from villin. *J. Mol. Biol. 249*, 1299–1310.
5. Kubelka, J., Eaton, W. A., and Hofrichter, J. (2003) Experimental tests of villin subdomain folding simulations. *J. Mol. Biol. 329*, 625–630.
6. McKnight, C. J., Doering, D. S., Matsudaira, P. T., and Kim, P. S. (1996) A thermostable 35-residue subdomain within villin headpiece. *J. Mol. Biol. 260*, 126–134.
7. Wang, M., Tang, Y., Sato, S., Vugmeyster, L., McKnight, C. J., and Raleigh, D. P. (2003) Dynamic NMR line-shape analysis demonstrates that the villin headpiece subdomain folds on the microsecond time scale. *J. Am. Chem. Soc. 125*, 6032–6033.
8. Doering, D. S., and Matsudaira, P. T. (1996) Cysteine scanning mutagenesis at 40 of 76 positions in villin headpiece maps the F-actin binding site and structural features of the domain. *Biochemistry 35*, 12677–12685.
9. Friederich, E., Vancompernolle, K., Huet, C., Goethals, M., Finidori, J., Vandekerckhove, J., and Louvard, D. (1992) An actin-binding site containing a conserved motif of charged amino acid residues is essential for the morphogenic effect of villin. *Cell 70*, 81–92.
10. Vermeulen, W., Vanhaesebrouck, P., Van Troys, M., Verschueren, M., Fant, F., Goethals, M., Ampe, C., Martins, J. C., and Borremans, F. A. (2004) Solution structures of the C-terminal headpiece subdomains of human villin and advillin, evaluation of headpiece F-actin-binding requirements. *Protein Sci. 13*, 1276–1287.
11. Chiu, T. K., Kubelka, J., Herbst-Irmer, R., Eaton, W. A., Hofrichter, J., and Davies, D. R. (2005) High-resolution X-ray crystal structures of the villin headpiece subdomain, an ultrafast folding protein. *Proc. Natl. Acad. Sci. U.S.A. 102*, 7517–7522.
12. McKnight, C. J., Matsudaira, P. T., and Kim, P. S. (1997) NMR structure of the 35-residue villin headpiece subdomain. *Nat. Struct. Biol. 4*, 180–184.
13. Vugmeyster, L., Trott, O., McKnight, C. J., Raleigh, D. P., and Palmer, A. G., III (2002) Temperature-dependent dynamics of the villin headpiece helical subdomain, an unusually small thermostable protein. *J. Mol. Biol. 320*, 841–854.
14. Yang, A. S., and Honig, B. (1993) On the pH dependence of protein stability. *J. Mol. Biol. 231*, 459–474.
15. Tang, Y., Grey, M. J., McKnight, J., Palmer, A. G., III, and Raleigh, D. P. (2006) Multistate folding of the villin headpiece domain. *J. Mol. Biol. 355*, 1066–1077.
16. Grey, M. J., Tang, Y., Alexov, E., McKnight, C. J., Raleigh, D. P., and Palmer, A. G., III (2006) Characterizing a partially folded intermediate of the villin headpiece domain under non-denaturing conditions: Contribution of His41 to the pH-dependent stability of the N-terminal subdomain. *J. Mol. Biol. 355*, 1078–1094.
17. Pardee, J. D., and Spudich, J. A. (1982) Purification of muscle actin. *Methods Enzymol. 85*, 164–181.
18. Edelhoch, H. (1948) (1967) Spectroscopic determination of tryptophan and tyrosine in proteins. *Biochemistry 6*, 1954.
19. Neuhoff, V., Arold, N., Taube, D., and Ehrhardt, W. (1988) Improved staining of proteins in polyacrylamide gels including isoelectric-focusing gels with clear background at nanogram sensitivity using Coomassie Brilliant Blue G-250 and R-250. *Electrophoresis 9*, 255–262.
20. Schägger, H., and von Jagow, G. (1987) Tricine−sodium dodecyl sulfate−polyacrylamide gel electrophoresis for the separation of proteins in the range from 1 to 100 kDa. *Anal. Biochem. 166*, 368–379.
21. Jones, T. A., Zou, J. Y., and Cowan, S. W. (1991) Improved methods for building protein models in electron density maps and the location of errors in these models. *Acta Crystallogr., Sect. A: Found. Crystallogr. 47* (part 2), 110–119.
22. Brünger, A. T., Adams, P. D., Clore, G. M., DeLano, W. L., Gros, P., Grosse-Kunstleve, R. W., Jiang, J. S., Kuszewski, J., Nilges, M., Pannu, N. S., Read, R. J., Rice, L. M., Simonson, T., and Warren, G. L. (1998) Crystallography and NMR system: A new

software suite for macromolecular structure determination. *Acta Crystallogr., Sect. D: Biol. Crystallogr. 54*, 905–921.
23. Chou, P. Y., and Fasman, G. D. (1978) Prediction of the secondary structure of proteins from their amino acid sequence. *Adv. Enzymol. Relat. Areas Mol. Biol. 47*, 45–148.
24. Chou, P. Y., and Fasman, G. D. (1978) Empirical predictions of protein conformation. *Annu. Rev. Biochem. 47*, 251–276.
25. Swillens, S. (1995) Interpretation of binding curves obtained with high receptor concentrations—Practical aid for computer analysis. *Mol. Pharmacol. 47*, 1197–1203.
26. Pelton, J. G., Torchia, D. A., Meadow, N. D., and Roseman, S. (1993) Tautomeric states of the active-site histidines of phosphorylated and unphosphorylated IIIGlc, a signal-transducing protein from *Escherichia coli*, using two-dimensional heteronuclear NMR techniques. *Protein Sci. 2*, 543–558.
27. Koradi, R., Billeter, M., and Wüthrich, K. (1996) MOLMOL: A program for display and analysis of macromolecular structures. *J Mol. Graphics 14*, 51–55.

BI7022738